Size-Dependent Magnetism of EuS Nanoparticles

Michelle D. Regulacio, Srotoswini Kar, Edward Zuniga, Guangbin Wang,[†] Norman R. Dollahon,[§] Gordon T. Yee,[†] and Sarah L. Stoll*

Department of Chemistry, Georgetown University, Washington, D.C. 20057

Received December 5, 2007. Revised Manuscript Received January 29, 2008

EuS nanoparticles were synthesized by solution-phase thermolysis of the diethylammonium salt of the anionic europium dithiocarbamate complex, $[Eu(S_2CNEt_2)_4]^-$. Oleylamine and triphenylphosphine were used as surfactants to prevent nanoparticle agglomeration and stabilize particle growth. By varying the synthetic parameters such as reaction temperature, heating time, and the [surfactant]:[precursor] ratio, nanoparticles of different sizes were obtained. The size-dependent magnetic properties of these nanoparticles were studied, and it was observed that a decrease in the ferromagnetic ordering temperature occurs with decreasing particle size.

Introduction

There has been a growing interest in magnetic nanoparticles due to their expanding number of potential applications, which include catalysis,[1,2] data storage,[3] medical imaging,[4] drug delivery,[5] biolabeling,[6] and bioseparation.[7] In many cases, the fundamental materials property important for applications is the magnitude of the nanoparticle saturation magnetization (M_s).[8] This is because many of the applications depend on magnetic filtration (i.e., the use of an external magnetic field to remove the magnetic nanoparticle from solution, along with anything bound to it).[9] However, the development of future generation of memory, sensor, and logic devices (e.g. magnetic random access memory, spin valves, and magnetic tunnel junctions)[10,11] will depend on tailored magnetic and electronic properties. Previous studies of magnetic nanoparticles have mainly focused on metallic (e.g., Fe, Co, Ni)[12–14] and insulating (e.g., Fe_2O_3, Fe_3O_4)[15,16] materials. Finite size effects in magnetic semiconductors, on the other hand, have been given far less attention. Nanoparticles of magnetic semiconductors have the potential to provide new insights into the details of the electronic band structure (sensitive to particle size) and how this influences basic magnetic properties of materials in confined geometries.

One reason magnetic semiconductors may not have been studied extensively is that there are few classes of materials that exhibit both intrinsic magnetic and semiconducting properties (as distinct from magnetic ion-doped II-VI or III-V semiconductors or "dilute magnetic semiconductors" which have been well investigated). One of the most important series of magnetic semiconductors is the europium chalcogenides, EuX (S = O, S, Se, Te), whose members exhibit magnetic ordering from ferromagnetism, metamagnetism to antiferromagnetism. Particular interest has been given to EuS, which displays great potential as material for optomagnetic and luminescent devices.[17–19] EuS is a narrow band gap ferromagnetic semiconductor (E_g = 1.65 eV) with a Curie temperature, T_c, of 16.6 K.[20] The relationship between electronic structure and magnetic properties in europium chalcogenides has been intensely investigated experimen-

* Author to whom correspondence should be addressed. E-mail: sls55@georgetown.edu. Fax: 202-687-6209. Tel.: 202-687-5839.

[†] Current address: Department of Chemistry, Virginia Polytechnic Institute and State University, Blacksburg, VA 24061.

[§] Current address: Department of Biology, Villanova University, Villanova, PA 19085.

(1) Hu, G.; Yee, G. T.; Lin, W. *J. Am. Chem. Soc.* **2005**, *127* (36), 12486–12487.
(2) Son, S. U.; Park, K. H.; Chung, Y. K. *J. Am. Chem. Soc.* **2002**, *124* (24), 6838–6839.
(3) Teng, X.; Yang, H. *J. Am. Chem. Soc.* **2003**, *125*, 14559–14563.
(4) Selvan, S. T.; Patra, P. K.; Ang, C. Y.; Ying, J. Y. *Angew. Chem., Int. Ed.* **2007**, *46*, 2448–2452.
(5) Kim, J.; Lee, J. E.; Lee, J.; Yu, J. H.; Kim, B. C.; An, K.; Hwang, Y.; Shin, C.-H.; Park, J.-G.; Kim, J.; Hyeon, T. *J. Am. Chem. Soc.* **2006**, *128* (3), 688–689.
(6) Horak, D.; Babic, M.; Jendelova, P.; Herynek, V.; Trchova, M.; Pientka, Z.; Pollert, E.; Hajek, M.; Sykova, E. *Bioconj. Chem.* **2007**, *18* (3), 635–644.
(7) Sen, T.; Sebastianelli, A.; Bruce, I. J. *J. Am. Chem. Soc.* **2006**, *128* (22), 7130–7131.
(8) Gu, H.; Xu, K.; Xu, C.; Xu, B. *Chem. Commun.* **2006**, 941.
(9) Bucak, S.; Jones, D.; Laibinis, P.; Hatton, T. A. *Biotechnol. Prog.* **2003**, *19*, 477.
(10) Bader, S. D. *Rev. Mod. Phys.* **2006**, *78*, 1.
(11) Krishnan, K. M.; Pakhomov, A.; Bao, Y.; Blomqvist, P.; Chun, Y.; Gonzales, M.; Griffin, K.; Ji, X.; Roberts, B. K. *J. Mater. Sci.* **2006**, *41*, 793.
(12) Burke, N. A. D.; Stover, H. D. H.; Dawson, F. P. *Chem. Mater.* **2002**, *14*, 4752–4761.
(13) Zalich, M. A.; Baranauskas, V. V.; Riffle, J. S.; Saunders, M.; St Pierre, T. G. *Chem. Mater.* **2006**, *18*, 2648–2655.
(14) Chen, D.-H.; Wu, S.-H. *Chem. Mater.* **2000**, *12*, 1354–1360.
(15) Hyeon, T.; Lee, S. S.; Park, J.; Chung, Y.; Na, H. B. *J. Am. Chem. Soc.* **2001**, *123*, 12798–12801.
(16) Sun, S.; Zeng, H. *J. Am. Chem. Soc.* **2002**, *124*, 8204–8205.
(17) Tanaka, K.; Tatehata, N.; Fujita, K.; Hirao, K. *J. Appl. Phys.* **2001**, *89* (4), 2213–2219.
(18) Muller, C.; Lippitz, H.; Paggel, J. J.; Fumagalli, P. *J. Appl. Phys.* **2004**, *95* (11), 7172–7174.
(19) Chen, W.; Zhang, X.; Huang, Y. *Appl. Phys. Lett.* **2000**, *76* (17), 2328–2330.
(20) Wachter, P. Europium Chalcogenides: EuO, EuS, EuSe and EuTe. In *Handbook on the Physics and Chemistry of Rare Earths*; Gschneider, K. A. J., Eyring, L. R., Eds.; North-Holland Publishing Company: Amsterdam, 1979; Vol. 2.
(21) Goncharenko, I. N.; Mirebeau, I. *Phys. Rev. Lett.* **1998**, *80* (5), 1082–1085.

10.1021/cm703463s CCC: $40.75
Published on Web 05/06/2008

tally[21] and theoretically.[22,23] We have been interested in this system as a model for understanding magnetic communication in magnetic semiconductors and lanthanide materials at nanoscale dimensions.

Magnetic nanoparticles have been investigated for the size dependence of a variety of magnetic properties including: domain structure, magnetic anisotropy, coercive field, and saturation magnetization.[24] Generally, it has been found that as the dimensions of the material are reduced there is a critical diameter where the formation of domain walls becomes unfavorable. This results in a single domain particle. With further size reduction, the nanoparticle progresses from single domain behavior to superparamagnetism as the magnetic anisotropy increases.[25] Also below the critical diameter, the coercive field increases as single domain particles are formed. However, for continued reduction in size, the coercive field falls to zero for superparamagentic nanoparticles.[26] The saturation magnetization decreases with decreasing size in insulating oxide nanoparticles but increases for metallic nanoparticles. The reduced coordination of surface atoms in metallic nanoparticles is thought to cause band narrowing resulting in an increased magnetic moment, whereas ionic compounds are thought to have disordered spins near the surface resulting in a reduced magnetic moment.[27] Finally, the reduced coordination number of the surface atoms can also manifest as a decrease in the ferromagnetic ordering temperature as observed in poly(vinylpyrrolidone)-capped nanoparticles of Prussian blue.[28] Magnetic semiconductors provide an interesting contrast to metallic and ionic materials because the magnetic communication is understood in terms of the electronic band structure, and depends significantly on the energy separation between the conduction and valence bands.

One advantage of using europium chalcogenides to study size-dependent magnetism is that the theory to explain magnetic ordering is well defined in this class of compounds.[29,30] The Curie temperature is a function of both coordination number and the size of the band gap, as seen in the equation,[20]

$$k_B\theta = \frac{2}{3}S(S+1)[Z_1J_1 + Z_2J_2] \quad (1)$$

where θ is the paramagnetic Curie temperature (For EuS, $T_C \sim 0.89\theta$, where T_C is the ferromagnetic Curie temperature),[20] k_B is Boltzmann's constant, $S = 7/2$ for the Eu^{2+} $4f^7(^8S_{7/2})$ ground state. The coordination number is taken into account in the term Z,[31] where for the nearest neighbors $Z_1 = 12$ and the next-nearest neighbors $Z_2 = 6$. The electronic band gap is found in J_1, which has the form $J_1 = Ab^2/E_g^2$, where A is a function of intra-atomic exchange (4f valence to 5d conduction band exchange, a measure of the extent of delocalization of f electrons in the conduction band), b is a measure of the orbital overlap, and E_g is the electronic energy band gap.[21] Thus, this system provides a simple theoretical framework to interpret magnetic properties as a function of particle size. As particle size is reduced, both the fraction of surface atoms with reduced coordination (Z) and the energy gap (E_g) should increase in a predictable way. The functional relationship of particle size with T_C should provide insight into the magnetic communication.

We have previously reported changes in the ferromagnetic ordering temperature for the EuS semiconductor nanoparticles relative to that of the bulk material.[32] In this work, we report the size-controllable synthesis of EuS nanoparticles, which are much smaller (<10 nm) than those we have previously studied. We provide structural, optical and magnetic characterization to evaluate the role of quantum confinement and surface effects on size-dependent magnetic properties.

Experimental Section

All chemicals were purchased from Aldrich Chemical Co. and used as received, unless otherwise noted.

Synthesis of $NH_2Et_2[Eu(S_2CNEt_2)_4]$. An isopropanol solution (15 mL) of diethylammonium diethyldithiocarbamate (0.89 g, 4.0 mmol) was added to an isopropanol solution (5 mL) of $Eu(NO_3)_3 \cdot 5H_2O$ (0.43 g, 1.0 mmol). Red-orange crystals precipitated immediately and were collected by vacuum filtration. IR (KBr, cm^{-1}): $\nu_{C-N} = 1484$(s), $\nu_{C-S} = 1004$(m). ^1H NMR: δ 1.49 (t, J = 7.2 Hz, 24H), δ 3.31 (q, J = 7.1 Hz, 16H). Resonance for the diethylammonium protons were not observed. λ_{max} (CH_3CN, nm): 267, 397, 422, 467, 534, 580. Anal. calcd. for $C_{24}H_{52}N_5S_8Eu$: C, 35.18; H, 6.40; N, 8.55. Found: C, 33.38; H, 5.94; N, 8.96. Percent yield 83%.

Solid-State Thermolysis 1. $NH_2Et_2[Eu(S_2CNEt_2)_4]$ (500 mg) was loaded in a quartz tube (2 cm × 20 cm) inside a glovebox and the system was placed under vacuum for 30 min prior to sealing and heating. Although the precursor is moisture and air stable, the thermolysis was carried out under vacuum to prevent the formation of surface Eu_2O_2S. The sealed tube was heated in a furnace at 500 °C for 3 h and was annealed at 700 °C for another 3 h, to enhance crystallinity (which increases with increasing temperature). Identical products based on X-ray powder diffraction were obtained for similar decompositions under conditions of flowing nitrogen or dynamic vacuum.

Solution-Phase Thermolysis 2. The two largest nanoparticles, 19.1 ± 0.2 nm (**2a**) and 14.6 ± 0.1 nm (**2b**), were synthesized and characterized as previously reported.[32] Briefly, the molecular precursor was dissolved in a mixture of trioctylphosphine and oleylamine and heated to 240 °C for 7.5 h (**2a**) and 300 °C for 30 min (**2b**), respectively.

Solution-Phase Thermolysis 3 and 4. $NH_2Et_2[Eu(S_2CNEt_2)_4]$ (0.50 g, 0.61 mmol) was dissolved in 6 mL (18.3 mmol) oleylamine (OA) resulting in a red-orange solution. In a three-neck flask, a mixture of 9.6 g (36.6 mmol) triphenylphosphine (TPP) and 6.00 mL (18.3 mmol) OA was heated to 280 °C under nitrogen. The total volume of OA used was 12 mL (36.6 mmol), giving an [OA]/[precursor] ratio of 60:1. The precursor solution was quickly injected to the hot solvent mixture and the temperature was maintained at 280 °C for 2 h. The color of the mixture immediately turned dark purple upon addition. After 30 min, the mixture was cooled to 70

(22) Maletta, H. *J. Appl. Phys.* **1982**, *3* (3), 2185.
(23) Kunes, J.; Ku, W.; Pickett, W. *J. Phys. Soc. Jpn.* **2005**, *74* (5), 1408.
(24) Leslie-Pelecky, D.; Rieke, R. *Chem. Mater.* **1996**, *8*, 1770.
(25) Lu, A.-H.; Salabas, E. L.; Schuth, F. *Angew. Chem., Int. Ed.* **2007**, *46*, 1222–1244.
(26) Spaldin, N. A. *Magnetic Materials: Fundamentals and Device Applications*; Cambridge University Press: New York, 2003.
(27) Kodama, R. H. *J. Magn. Magn. Mater.* **1999**, *200*, 359.
(28) Uemura, T.; Kitagawa, S. *J. Am. Chem. Soc.* **2003**, *125*, 7815.
(29) Nolting, W. *J. Phys. C: Solid State Phys.* **1982**, *15*, 733–745.
(30) Rhyne, J. J.; McGuire, T. R. *IEEE Trans. Magn.* **1972**, *8* (1), 105.
(31) McGuire, T. R.; Shafer, M. W. *J. Appl. Phys.* **1964**, *35*, 984–988.
(32) Regulacio, M. D.; Bussmann, K.; Lewis, B.; Stoll, S. L. *J. Am. Chem. Soc.* **2006**, *128* (34), 11173–11179.

°C. Ethanol (100 mL) was then added to precipitate out the nanoparticles. The purple-black solid (**3a**) was isolated by centrifugation and was then redispersed in heptane yielding a dark purple solution. The nanoparticle solution was centrifuged, and the small amount of solid that settled was discarded. Methanol was added to the dark purple supernatant and caused the nanoparticles to precipitate. Subsequently, the nanoparticles were isolated by centrifugation, washed with MeOH, and dried in nitrogen atmosphere. The effect of varying the heating time was studied by repeating this experiment with heating times of 60 (**3b**), 30 (**3c**), and 15 (**3d**) min.

The effect of varying the reaction temperature was also studied by repeating this experiment at 200 °C for 30 min (**4a**). To study the effect of the [OA]/[precursor] ratio, a ratio of 100:1 was also used (**4b**) for $T = 280$ °C and 30 min. Finally, the experiment was repeated with just OA as the solvent (no TPP) (**4c**) for $T = 280$ °C and 30 min.

Characterization. The precursor, $NH_2Et_2[Eu(S_2CNEt_2)_4]$ was characterized by elemental analysis, IR, NMR and UV−vis spectroscopy. Infrared spectra were measured in the range 450−4000 cm^{-1} as pressed pellets in KBr on a Perkin-Elmer Spectrum One FTIR spectrometer. NMR spectra were recorded using a 300 MHz Varian spectrometer, calibrated internally to residual solvent for ^1H in $CDCl_3$. Absorption spectra were recorded from 210−800 nm in acetonitrile on an HP UV−vis spectrometer. Elemental analysis (C, H and N content) were performed on a Perkin-Elmer PE 2400 microanalyzer. Thermal analysis was performed on an SDT Q600 TA instrument. Simultaneous TGA-DTA data were studied from samples in an alumina pan from 25−1000 °C under a N_2 flow of 50 mL/min. The heating rate was initially set at 10 °C/min and was changed to 20 °C/min when the temperature went beyond 600 °C.

Nanoparticles were characterized by transmission electron microscopy (TEM) images recorded using a Hitachi H-7600 TEM equipped with an AMT XR 40B camera and operated at 100 kV. Samples were prepared by dropping 3-μL heptane solutions of nanoparticles onto carbon-coated copper TEM grids.

Further structural characterization was done using X-ray powder diffraction using a Rigaku RAPID Curved IP X-ray powder diffractometer with Cu Kα radiation and an image plate detector. Rietveld refinement was performed with the general structure analysis system (GSAS)[33] using the EXPGUI graphical user interface.[34] Literature values for atomic positions, space group, temperature factor, and cell dimensions for EuS were used.[35] Bulk EuS material was used as a standard to determine instrument strain broadening. The refinement process involved refining the background (using a shifted Chebyschev polynomial), scale factor, and profile function 3. Profile coefficients were optimized using bulk EuS. The powder diffraction data of nanoparticles were refined using these parameters as fixed, with the only variables: the Lorentzian microstrain (Ly), Lorentzian microstrain anisotropy (ptec), Lorentzian particle size (Lx), Lorentzian particle-size anisotropy (stec), and shift (shft) coefficients. The final refinement of 5 variables (plus background and scale factor variables) using 6800 observations gave residuals that ranged from wR 0.0293−0.0031.

Absorption spectra of the nanoparticles were recorded from 250−800 nm on an HP UV−visible spectrometer. To determine the optical band gaps, a plot of the square root of the product of the absorption coefficient and energy, $(\alpha E)^{1/2}$, as a function of energy was used.[36] The optical band gap was taken as the energy where the absorption extrapolates to zero from the linear portion of the absorption edge.

Magnetic Measurements. Magnetic measurements were performed on a 7 T Quantum Design MPMS SQUID magnetometer. Measurements of magnetization as a function of temperature were performed for zero-field-cooled samples, then increasing the temperature from 1.8 to 300 K in a field of 500 Oe. Hysteresis curves were measured at 1.8 K. Samples were packed between cotton plugs, placed inside gelatin capsules, cooled in a zero applied field, and measured upon warming. Diamagnetic corrections were applied on the basis of Pascal's constants. The data were corrected for the diamagnetism of the gel cap and the cotton plug.

Results and Discussion

Synthesis. The synthetic method used to form magnetic nanoparticles is extremely important in determining properties because the size, shape, and surface properties all have a profound influence over magnetic measurements.[37,38] The synthetic criteria for nanoparticles includes: high phase purity, monodispersity, and easily controllable surface derivatization. Previously, EuS nanoparticles have been prepared by solid-state diffusion of powdered EuS into the pores of zeolites,[19] formation in liquid ammonia solutions,[39–41] and white LED[42] and microwave[43] irradiation of single-source precursors resulting in uncapped nanoparticles. On the other hand, thermal decomposition of molecular precursors in suitable coordinating solvents has been reported to produce capped nanoparticles of EuS.[32,44–46]This approach involves the design of a single-source precursor molecule with the composition of the target material, and with a relatively low decomposition temperature for solution thermolysis. Europium(III) dithiocarbamate complexes with 1,10-phenanthroline (phen) or 2,2′-bipyridine (bipy) ligands, $Eu(S_2CNR_2)_3L$ (where R = alkyl group; L = phen or bipy), have been the precursor of choice in the solution-phase thermolysis approach of preparing nanocrystalline EuS. These complexes are monomeric, air- and moisture-stable and are known to decompose to EuS via an internal redox reaction.[47] Size control in similar nanoparticle synthesis was achieved by varying the concentration of the $Eu(S_2CN(Et)_2)_3L$ precursor in oleylamine.[46] However, the presence of chelating ligands (phen or bipy) is believed to interfere with nanocrystal growth. When

(33) Larson, A. C.; Von Dreele, R. B. *General Structure Analysis System (GSAS)*; Report LAUR 86-748, Los Alamos National Laboratory: Los Almos, NM, 2004.
(34) Toby, B. H. *J. Appl. Crystallogr.* **2001**, *34*, 210–213.
(35) Wachter, P. *CRC Crit. Rev. Solid State Sci.* **1972**, *3*, 189–238.
(36) Holonyak, N. *Optical Processes in Semiconductors*; Prentice-Hall, Inc.: New Jersey, 1971.
(37) Song, Q.; Zhang, Z. J. *J. Am. Chem. Soc.* **2004**, *126*, 6164.
(38) Iglesias, O.; Labarta, A. *Physica B* **2004**, *343*, 286.
(39) Thongchant, S.; Hasegawa, Y.; Wada, Y.; Yanagida, S. *J. Phys. Chem. B* **2003**, *107*, 2193–2196.
(40) Thongchant, S.; Hasegawa, Y.; Wada, Y.; Yanagida, S. *Chem. Lett.* **2003**, *32* (8), 706–707.
(41) Kataoka, T.; Tsukahara, Y.; Hasegawa, Y.; Wada, Y. *Chem. Commun.* **2005**, 6038–6040.
(42) Hasegawa, Y.; Afzaal, M.; O'Brien, P.; Wada, Y.; Yanagida, S. *Chem. Commun.* **2005**, 242–243.
(43) Hasegawa, Y.; Okada, Y.; Kataoka, T.; Sakata, T.; Mori, H.; Wada, Y. *J. Phys. Chem. B* **2006**, *110*, 9008–9011.
(44) Mirkovic, T.; Hines, M. A.; Nair, P. S.; Scholes, G. D. *Chem. Mater.* **2005**, *17*, 3451–3456.
(45) Zhao, F.; Sun, H.-L.; Gao, S.; Su, G. *J. Mater. Chem.* **2005**, *15*, 4209–4214.
(46) Zhao, F.; Sun, H.-L.; Su, G.; Gao, S. *Small* **2006**, *2* (2), 244–248.
(47) Regulacio, M. D.; Tomson, N.; Stoll, S. L. *Chem. Mater.* **2005**, *17* (12), 3114–3121.

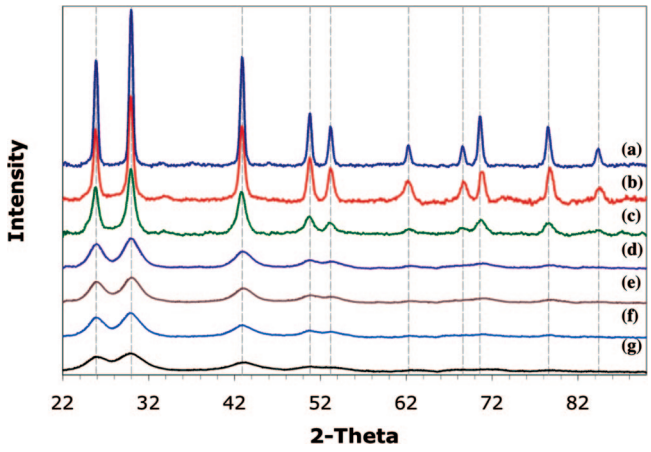

Figure 1. PXRD patterns of EuS prepared by (a) solid-state decomposition of $NH_2Et_2[Eu(S_2CNEt_2)_4]$ (sample 1); solution thermolysis of $Eu(S_2CN^tBu_2)_3$phen as previously reported, (b) sample **2a**, 19.1 ± 0.2 nm, and (c) sample **2b**, 14.6 ± 0.1 nm; solution thermolysis of $NH_2Et_2[Eu(S_2CNEt_2)_4]$ with heating times of (d) 120 min (sample **3a**, 7.2 ± 0.9 nm), (e) 60 min (sample **3b**, 6.2 ± 0.6 nm), (f) 30 min (sample **3c**, 5.7 ± 0.7 nm), and (g) 15 min (sample **3d**, 4.9 ± 0.6 nm).

surface-bound, these ligands also interfere with the optical spectrum of the nanoparticles.[44] For these reasons, the diethylammonium salt of the anionic tetrakis complex, $[Eu(S_2CNEt_2)_4]^-$, was used as the molecular precursor in this study. Thermogravimetric analysis (see Figure S1 in the Supporting Information) reveals that this complex decomposes in the temperature range of 115−340 °C, which is much lower than the decomposition temperature observed for the neutral mixed-ligand complexes with phen[47] or bipy.[46] The remaining weight after decomposition corresponded to a mass of 1 Eu and 1 S, supporting the formation of EuS. To further confirm the utility of this precursor in the synthesis of EuS, solid-state thermolysis was performed, and the black solid that remained was analyzed by powder X-ray diffraction (PXRD). Figure 1a shows the PXRD pattern of the highly crystalline decomposition product. All diffraction peaks are indexed to cubic EuS.

In preparing the EuS nanoparticles, we have employed the most commonly used injection-based approach in nanoparticle synthesis. The precursor is readily soluble in OA at ambient temperature and was rapidly added as a precursor−OA solution into a vessel containing a hot mixture of OA and TPP. The temperature is high enough to instantly decompose the precursor, resulting in supersaturation of species in solution, causing immediate nucleation of the nanoparticles. The effect of synthetic conditions on particle size were investigated for: varying the heating time, the reaction temperature and the [OA]/[precursor] ratio, as well as the effect of using only OA (no TPP) as the coordinating solvent. Representative TEM images of the particles obtained under different reaction conditions are shown in Figure 2 (histograms are shown in Figure S2), and the average sizes of these particles are summarized in Table 1.

Generally, we found that increasing the reaction time results in larger average particle size (consistent with Ostwald ripening). From the TEM image of particles grown for the longest time, 120 min (Figure 2a, sample **3a**), it can be observed that some of the particles began to coagulate, resulting in a wider size distribution. In addition to TEM, the X-ray powder diffraction patterns of the particles prepared with varying heating times are shown in Figure 1. The patterns confirm that the nanoparticles produced are single phased EuS, and as the particle size decreases the diffraction peaks broaden, as expected. Lowering the injection temperature from 280 to 200 °C gave larger particles. We interpret this as due to rapid precursor decomposition at high temperatures which results in higher nuclei concentration, leading to smaller average particle size. Interestingly, in this work, well-separated particles were still obtained at temperatures as low as 200 °C. This is in contrast to previous studies where flowerlike aggregates of EuS particles were obtained when the reaction temperature is set below 260 °C for the mixed-ligand precursor.[45,46] Increasing the [OA]/[precursor] ratio to 100:1 gave smaller particles. Besides their usual role as capping agents in nanoparticle synthesis, alkylamines are also known to lower the decomposition temperature of molecular precursors. The use of alkylamines in promoting the thermolysis of metal xanthate and metal dithiocarbamate precursors (metal = Cd, Zn, Pb, Hg, Ni, Cu, Mn) by providing a new decomposition route has been previously studied by Pradhan et al.[48] They have found that primary alkylamines significantly lowered the decomposition temperature of metal xanthates from 140 to 70 °C and that of metal dithiocarbamates from 170 to 125 °C. Thus, increasing the amine concentration hastens the degradation process and favors the formation of more small nuclei. The formation of smaller particles with increasing amine concentration has been previously observed for Ag_2Se nanocrystals.[49] The use of both TPP and OA as capping ligands gave smaller nanoparticles relative to those produced with the absence of TPP. It is possible that the adsorption of bulky ligands to the surface of the nanocrystals slows the rate of addition of material to the nanoparticle, resulting in smaller average particle size.

Structure Analysis. We have used both TEM and PXRD to determine the size and structure of the EuS nanoparticles. For the nanoparticles smaller than 10 nm, the line broadening was significant enough to make it impractical to use the Scherrer equation (previously, for the 19.1- and 14.6-nm particles we have used the fwhm of the (111), (200), and (220) peaks).[32] Using GSAS Reitveld refinement the particle sizes were determined to be within 1−3% of the values determined from TEM, with the exception of the 7.2 ± 0.9 nm nanoparticles based on TEM which refined to a value of 9.2 nm ± 0.6 in GSAS. Disagreement between sizes obtained from XRD and TEM has been previously observed,[50] although, more typically, TEM overestimates particle size (due to agglomeration effects). Counting statistics are also important for making TEM meaningful, whereas XRD provides an average for the entire sample.

We were interested in determining the degree of strain in our nanoparticles, because previous work on EuS−PbS multilayers found changes in the ferromagnetic Curie tem-

(48) Pradhan, N.; Katz, B.; Efrima, S. *J. Phys. Chem. B* **2003**, *107* (50), 13843–13854.
(49) Ng, M. T.; Boothroyd, C.; Vittal, J. *J. Chem. Commun.* **2005**, *30*, 3820–3822.
(50) Nanda, J.; Sapra, S.; Sarma, D. **2000**, *12*, 1018.

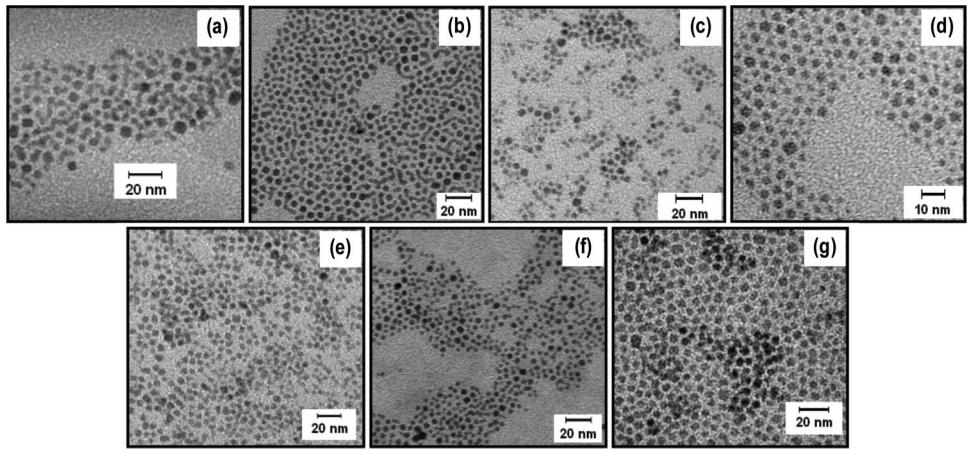

Figure 2. TEM images of EuS nanoparticles prepared at (a−d) 280 °C with [OA]/[precursor] and [TPP]/[precursor] = 60:1 and heating times of (a) 120 min (sample **3a**, 7.2 ± 0.9 nm), (b) 60 min (sample **3b**, 6.2 ± 0.6 nm), (c) 30 min (sample **3c**, 5.7 ± 0.7 nm), and (d) 15 min (sample **3d**, 4.9 ± 0.6 nm); (e) 200 °C for 30 min with [OA]/[precursor] and [TPP]/[precursor] = 60:1 (sample **4a**, 6.5 ± 0.6 nm); (f) 280 °C for 30 min with [OA]/[precursor] = 100:1 and [TPP]/[precursor] = 60:1 (sample **4b**, 4.9 ± 0.5 nm); and (g) 280 °C for 30 min with [OA]/[precursor] = 100:1 and no TPP (sample **4c**, 6.6 ± 0.6 nm).

Table 1. Summary of the Average Particle Size of EuS Obtained under Different Reaction Conditions

		reaction temperature (°C)	[OA]/[precursor] molar ratio	heating time (mins)	average particle size (nm)
[TPP]/[precursor]	**3a**	280	60:1	120	7.2 ± 0.9
molar	**3b**	280	60:1	60	6.2 ± 0.6
ratio = 60:1	**3c**	280	60:1	30	5.7 ± 0.7
	3d	280	60:1	15	4.9 ± 0.6
	4a	200	60:1	30	6.5 ± 0.6
	4b	280	100:1	30	4.9 ± 0.5
no TPP	**4c**	280	100:1	30	6.6 ± 0.6

perature attributed to substrate induced strain due to differences in the thermal expansion coefficients of the substrate and multilayer.[51] Strain in nanoparticles has been most commonly measured using EXAFS because of the advantages of this technique in determining first-neighbor distances, and its sensitivity to local structure about one type of atom.[52] For II-VI semiconductors, the surface interatomic distances differed from the bulk by <1.0%.[53] Using Raman scattering on similar materials in nanocrystalline thin films a peak shift was found to increase with decreasing particle size (associated with an increase in strain).[54] Although analysis of surface effects in small nanoparticles using structural refinement of X-ray powder diffraction data is best considered qualitative, we have used GSAS to estimate trends in strain as a function of particle size. Although this approach is successful for determining strain in microcrystalline powders[55] typically giving values less than 2%, we found that strain effects in nanoparticles using this method increased from 0.46% up to as high as 9.5% for the smallest nanoparticles (4.9 nm). These values appear unrealistically high. It is likely that determining strain requires the resolution of synchrotron radiation.[56] We did not refine on lattice parameters, which is likely to reduce the percent strain. Thermal effects can also contribute to the broadening of the X-ray diffraction pattern,[57] as well as defects or distortions of the lattice. More importantly, there is no clear method to include the particle size distribution in the simulated patterns. Using atomic pair distribution function analysis, which is a full-profile refinement method like GSAS, Kanatzidis and co-workers have determined size-dependent strain in CdSe to reach 0.5% for the smallest nanoparticle of 2 nm.[58] This appears to be the optimal method for determining strain in nanoparticles and will be used in future work.

Electronic Absorption. The dependence of energy gap, E_g, on particle size in semiconductor nanocrystals has been extensively studied.[59,60] Particles whose dimension becomes comparable to the bulk exciton Bohr radius, a_B, are observed to exhibit quantum confinement effects, which result in increasing the energy gap with decreasing particle size. Confinement effects in semiconductors are strong for particles with radius, r, that are significantly smaller than the exciton Bohr radius ($r \ll a_B$), intermediate for those with $r \sim a_B$ and weak for particles that are small but with radius that are still a few times larger than a_B ($r \gg a_B$). The bulk exciton Bohr radius is typically calculated using the equation,

$$a_B = a_0 \varepsilon \left(\frac{m_0}{\mu}\right) \qquad (2)$$

where a_0 is the hydrogen atom Bohr radius (~0.529 Å), ε is the optical dielectric constant of the material, m_0 is the free electron mass, and μ is the exciton reduced mass (Note that

(51) Stachow-Wojcik, A.; Story, T.; Dobrowolski, W.; Arciszewska, M.; Galazka, R. R.; Kreijveld, M. W.; Swuste, C. H. W.; Swagten, H. J. M.; de Jonge, W. J. M.; Twardowski, A.; Sipatov, A. Y. *Phys. Rev. B* **1999**, *60* (22), 15220–15229.
(52) Marcus, M.; Flood, W.; Steigerwald, M.; Brus, L.; Bawendi, M. *J. Phys. Chem.* **1991**, *95*, 1572.
(53) Herron, N.; Calabrese, J. C.; Farneth, W. E.; Wang, Y. *Science* **1993**, *259*, 1426.
(54) Chaure, S.; Chaure, B. B.; Pandey, R. K. *Physica E* **2005**, *28*, 439.
(55) Sutter, B.; Ming, D. W.; Clearfield, A.; Hossner, L. R. *Soil Sci. Soc. Am. J.* **2003**, *67*, 1935.
(56) Palosz, B.; Grzanka, E.; Gierlotka, S.; Stel'makh, S.; Pielaszek, R. P.; Bismayer, U.; Neuefeind, J.; Weber, H.-P.; Palosz, W. *Acta Phys. Pol., A* **2002**, *102* (1), 57.
(57) Guinier, A. *X-ray Diffraction*; Freeman: San Francisco, CA, 1963.
(58) Masadeh, A. S.; Bozin, E. S.; Farrow, C. L.; Paglia, G.; Huhas, P.; Billinge, S. J. L.; Karkamkar, A.; Kanatzidis, M. G. *Phys. Rev. B* **2007**, *76*, 115413.
(59) Trindade, T.; O'Brien, P.; Pickett, N. L. *Chem. Mater.* **2001**, *13*, 3843–3858.
(60) Brus, L. E. *J. Chem. Phys.* **1984**, *80* (9), 4403.

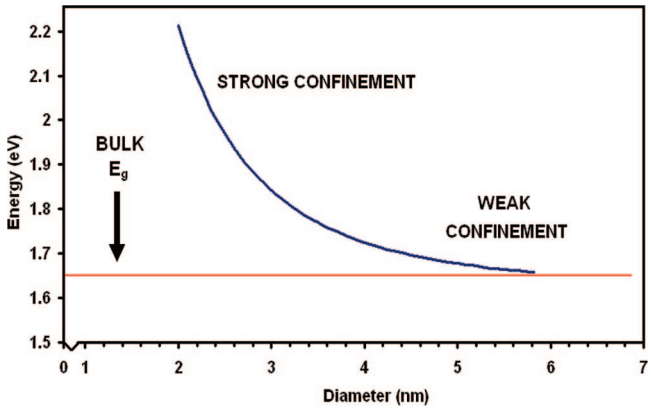

Figure 3. Size dependence of band gap for EuS calculated using Brus equation.

$\mu^{-1} = m_e^{*-1} + m_h^{*-1}$, where m_e^* and m_h^* are the effective mass of the electron and hole, respectively).[61] Using this formula and assuming that m_h^* is much larger than m_e^* (m_h^{*-1} is neglected), the exciton Bohr radius for EuS (ε is 10 and m_e^*/m_0 is 0.456)[62] is estimated as ~1.2 nm (or nanoparticle diameter of 2.4 nm).

The effect of quantum confinement is evident from the absorption spectrum of the material. For example in the case of CdSe with a direct bandgap semiconductor with E_g of 1.74 eV, the absorption edge shifts to higher energy (shorter wavelength) when the particle radius is comparable to the exciton Bohr radius of ~5.6 nm.[63–65] The relationship between particle size and E_g is given by the Brus equation,[60,66]

$$E_g^* = E_g + \left(\frac{\hbar^2\pi^2}{2\mu r^2}\right) - \left(\frac{1.8e^2}{4\pi\varepsilon_0\varepsilon r}\right) + \text{smaller terms} \qquad (3)$$

where E_g^* is the energy gap for particle with radius r, E_g is the bulk semiconductor band gap, $\hbar$ is the reduced Planck constant, e is the elementary charge, and ε_0 is the vacuum permittivity. The second term on the right refers to the quantum energy of localization and is inversely proportional to the square of the particle radius. The third term describes the Coulomb electron−hole interaction, which increases with $1/r$. Smaller terms, which take into account surface polarization effects, are also inversely proportional to r but are usually ignored. This equation describes the asymptotic approach of E_g^* to the bulk band gap and is valid for sufficiently small r. For EuS, E_g^* nears the bulk band gap for diameter larger than ~6 nm ($r \sim 3$ nm) as shown in Figure 3. Moreover, it can be observed from Figure 3 that strong confinement is exhibited by particles with diameter less than ~3 nm ($r \sim 1.5$ nm), and this is consistent with strong confinement effects for particles with $r \ll a_B$ (vide supra). Unfortunately, the smallest average particle diameter prepared in this work is 4.9 nm ($r = 2.45$ nm), which falls in the weak confinement regime.

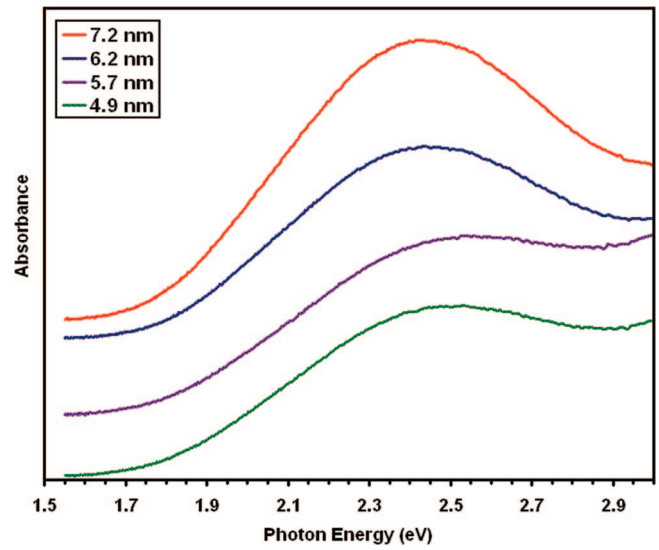

Figure 4. Absorption spectra of EuS nanoparticles of varying sizes.

Two major peaks dominate the absorption spectra of europium chalcogenides (see Supporting Information Figure S3).[67] The low-energy absorption peak has been assigned to the $4f^7(^8S_{7/2}) \rightarrow 4f^6(^7F_J)5d(t_{2g})^1$ transition whereas the high-energy absorption peak is attributed to the $4f^7(^8S_{7/2}) \rightarrow 4f^6(^7F_J)5d(e_g)^1$ transition and to an electronic charge transfer from the anion (Q^{2-}) to the cation (Eu^{2+}) (Figure S4). On the basis of transmission measurements on EuS thin films at 300 K performed by Guntherodt et al., the first peak is centered at 2.4 eV (~517 nm) while the second peak is situated at around 4.6 eV (~270 nm).[67] The onset of the first absorption peak is at 1.65 eV, which corresponds to the E_g of bulk EuS. Previous reports of EuS nanoparticles have identified a weak, broad peak that shifts in energy from 630 to 515 nm for nanoparticles ranging in size from 36 to 7 nm and identified this as the $4f^7(^8S_{7/2}) \rightarrow 4f^6(^7F_J)5d(t_{2g})^1$ transition.[40,41] We have also observed this peak at ~520 nm (~2.4 eV) for 19.1-nm nanoparticles.[32]In this work (Figure 4), we have observed a shift from 511 nm (2.43 eV) for the 7.2-nm particles down to 490 nm (2.53 eV) for the 4.9-nm nanoparticles. A corresponding shift in the band gap, as determined from the $(Abs*E)^{1/2}$-vs-energy plots, was observed. The blue-shifting of the absorption edge is indicative of quantum confinement, and the very small shift is expected for particles whose size falls in the weak confinement limit.

Magnetic Properties. The temperature-dependence of magnetic susceptibility was measured for five samples of varying particle size and the plots are shown in Figure 5. The ferromagnetic to paramagnetic transition becomes less pronounced as the particles size decreases. Others have observed a peak in the ZFC magnetization for nanoparticles smaller than 8 nm,[46] indicative of superparamagnetism which is not evident in our data. We believe our nanoparticles do not exhibit superparamagnetism, as supported by the small but measurable hysteresis in the M-vs-H curves (ranging from ~10 G for 7.2-nm nanoparticles down to ~3 G for the smallest nanoparticles,

(61) Klingshirn, C. *Semiconductor Optics*, 2nd ed.; Springer: Berlin, 2005.
(62) Umehara, M. *Phys. Rev. B* **2002**, *65*, 205208.
(63) Murray, C. B.; Norris, D. J.; Bawendi, M. G. *J. Am. Chem. Soc.* **1993**, *115*, 8706–8715.
(64) Cumberland, S. L.; Hanif, K. M.; Javier, A.; Khitrov, G. A.; Strouse, G. F.; Woessner, S. M.; Yun, C. S. *Chem. Mater.* **2002**, (14), 1576–1584.
(65) Chaure, S.; Chaure, N. B.; Pandey, R. K. *Physica E* **2005**, *28*, 439–446.
(66) Brus, L. E. *J. Phys. Chem.* **1986**, *90*, 2555–2560.
(67) Guntherodt, G.; Schoenes, J.; Wachter, P. *J. Appl. Phys.* **1970**, *41* (3), 1083–1084.

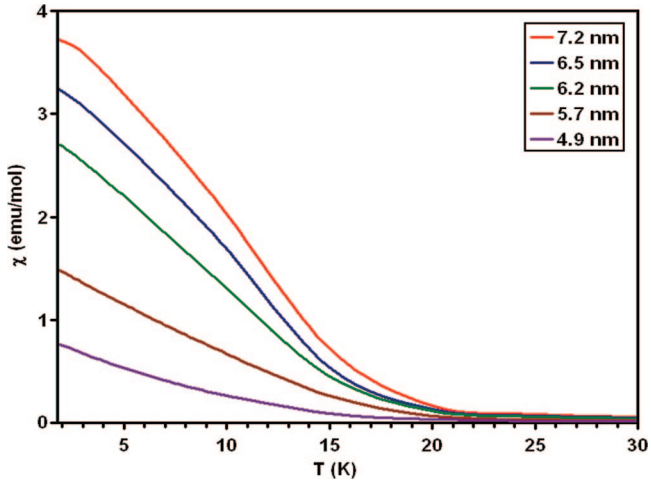

Figure 5. Temperature dependence of magnetization (χ) after zero-field-cooled magnetization using 500 Oe.

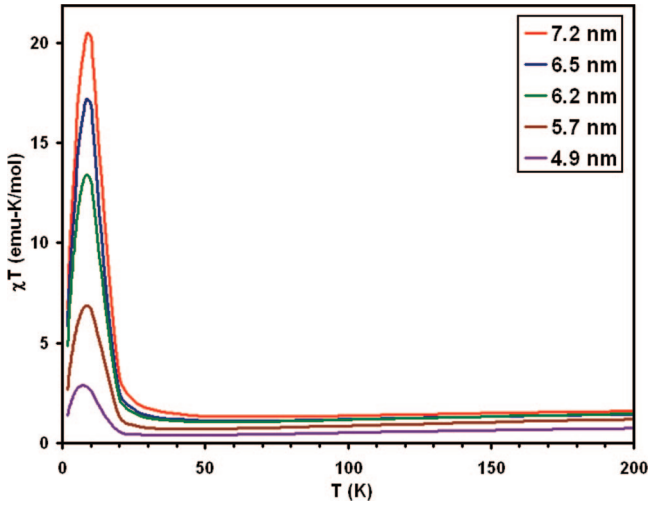

Figure 6. Temperature dependence of χT at 500 Oe.

4.9 nm). The decrease in coercive field with particle size suggests that we are below the critical diameter. The product of χT is plotted against temperature, and the curves are shown in Figure 6. The rapid rise in χT as the temperature is cooled below ~20 K, observed for all samples, is indicative of the onset of ferromagnetic interactions. The value of χT reaches a maximum and then rapidly decreases below T_C as a result of moment saturation.

An estimate of the Curie temperature through extrapolation from the χ-vs-T curves does not provide an unambiguous determination. For a more sensitive and accurate measure of T_C, we have made use of Arrott plots (i.e., magnetic isotherms).[68,69] This interpolation technique can be derived from either a Landau description of magnetization[70] or a power series expansion of the Brillouin function[68] and is valid only in the vicinity of the Curie temperature. Magnetic isotherms are plots of M^2 as a function of H/M at constant

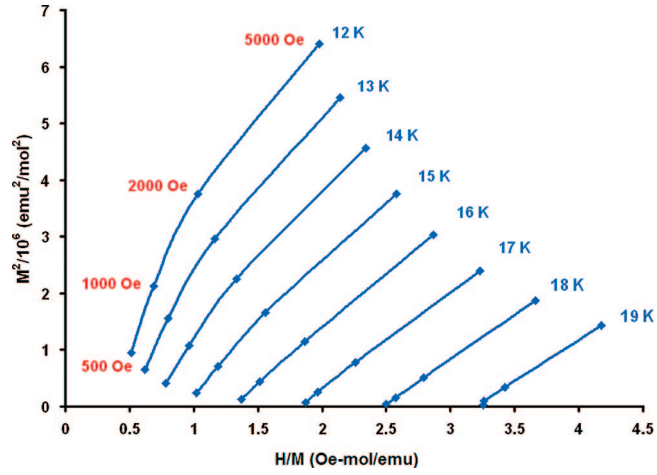

Figure 7. Arrott plot for 4.9 nm particles.

temperature (as seen in Figure 7 for 4.9 nm particles), and are based on the linear equation,

$$(H/M) = a(T - T_C) + bTM^2 \quad (4)$$

where H is the applied magnetic field, M is magnetization, T is temperature, and a and b are constants. Rearrangement of the equation gives,

$$M^2 = A(H/M) + B(T_C - T) \quad (5)$$

where $A = 1/bT$ and $B = a/bT$. These isotherms usually bend at temperatures below T_C at low fields due to magnetic anisotropy.[71] Since M is considered as the magnetization of material when domain alignment is complete, the low-field data can be ignored.[68] The intercept of these isotherms with the H/M-axis (i.e., where $M^2 = 0$) should be positive if $T > T_C$ and negative if $T < T_C$. This can be seen qualitatively in Figure 7, where the high-field data for $T = 12$ and 13 K have a negative x-intercept and those for $T = 14$ to 19 K have a positive x-intercept placing T_C between 13 and 14 K.

The spontaneous magnetization, M_s, is defined as the magnetization of the material at zero applied magnetic field. Thus, the intercept of the isotherms with the M^2-axis (i.e., where $H/M = 0$) corresponds to the square of the spontaneous magnetization, M_s^2. For the low-temperature isotherms where bending at low fields is observed, the y-intercept is typically extrapolated from the high-field region. At zero field, eq 5 becomes

$$M_s = B(T_C - T) \quad (6)$$

The M_s^2 of each isotherm is plotted against temperature (as shown in Figure 8 for 4.9-, 5.7-, and 7.2-nm particles), and the temperature where M_s^2 is zero (where the plot crosses the x-axis) gives the Curie temperature, T_C. For the 4.9-nm particles, a T_c of 13.2 K was observed. Using the same technique, the T_C for particles having an average size of 5.7 and 7.2 nm were found to be 13.8 and 14.3 K, respectively. This supports the earlier observation that the magnetic transition temperature decreases with particle size.[32]

In fact, the magnetic data from three previous studies of EuS can be interpreted as a decrease in ordering

(68) Aharoni, A. *Introduction to the Theory of Ferromagnetism*; Oxford University Press Inc.: New York, 1996; Vol. 93, p 80.
(69) Chikazumi, S. *Physics of Ferromagnetism*; Oxford University Press Inc.: New York, 1997; Vol. 94, p 123.
(70) Neumann, K.-U.; Ziebeck, K. R. A. *J. Magn. Magn. Mater.* **1995**, *140−144*, 967–968.
(71) Arrott, A.; Noakes, J. E. *Phys. Rev. Lett.* **1967**, *19* (14), 786–789.

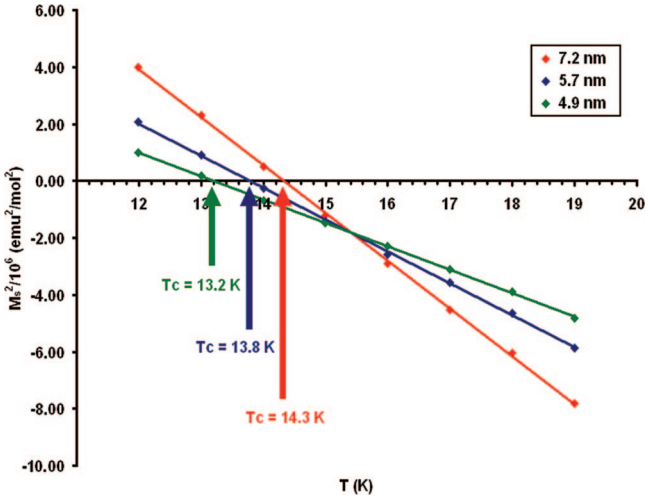

Figure 8. Curie temperature of EuS nanoparticles with average particle diameter of 7.2, 5.7, and 4.9 nm.

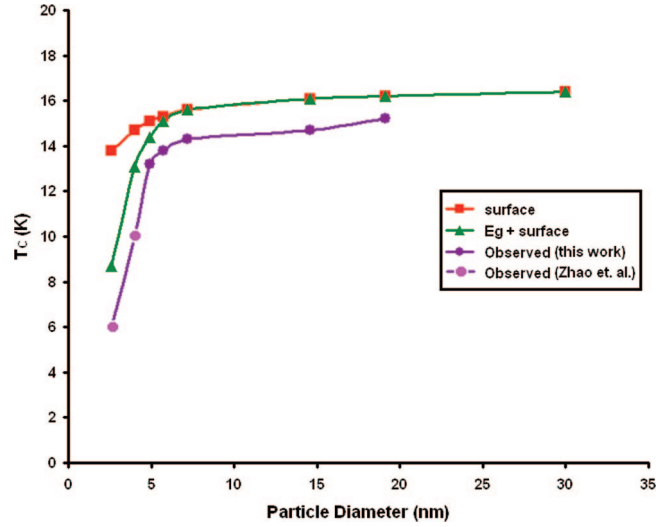

Figure 9. Calculated T_c-vs-particle size for calculated changes in surface coordination, E_g and surface coordination, and experimental data.

temperature with a decrease in size. The first example reported was for uncapped EuS nanoparticles prepared by thermolysis of precursors and then exposed to air.[45] Samples with increasing exposure to oxygen (1 h, 1 day, 1 week, and 1 month), based on extrapolation of their χ-vs-T data, have ordering temperatures that range from 15 down to ~7 K. Nanocrystals prepared under almost identical conditions, but open to air, formed Eu_2O_2S nanoparticles.[72] This suggests that the surface of the EuS nanoparticles previously reported were slowly oxidized to form a shell of Eu_2O_2S, effectively reducing the core diameter. The extent of this would be difficult to quantify but is consistent with decreasing T_C with particle size. However, a second example of capped, size-selected nanoparticles of EuS also exhibit a decrease in T_C as the particle size is reduced, down to ~6 K for the smallest sample, 2.6 nm (based on extrapolation from the published χ-vs-T curve).[46] The third example can be found in thin films of EuS−PbS multilayers, which noted a shift to lower T_C with a decrease in film thickness. For multilayers with 16 monolayers of EuS down to 3 monolayers of EuS, the ordering temperature decreased from 14 down to 8 K, respectively.[51] In this case, the model used to interpret the change in the ferromagnetic ordering temperature was described as the "bond-loss", which is effectively using eq 1, only taking into account the reduced coordination of surface Eu atoms in Z_1 and Z_2.

We have previously noted that there are only three possible mechanisms for the reduction of T_C with particle size: strain (deviations in Eu−S bond lengths would effect J_1 through changes to both E_g and orbital overlap, b), surface effects (i.e., reduced coordination of Eu), and energy band gap effects.[32] These different mechanisms can be distinguished by the functional relationship between E_g and particle size. We have neglected the effect of strain because our analysis does not conclusively determine the extent of strain, and the effects are ambiguous because changes in the Eu−S bond lengths should have opposite effects on E_g and b, and it is unclear how to measure b. We believe that both reduced coordination of surface atoms and band gap effects are required to closely model the changes in the ordering temperature with particle size. In Figure 9, we first plot the decrease in T_C for decreasing particle size taking into account only the reduction in coordination number (Z_1, Z_2 in eq 1). For each particle size, we calculated the fraction of surface atoms and estimated that the surface atoms would have half the coordination number of core atoms. The $1/r$ dependence of surface atoms (r being the radius of the particle) is evident in this graph. By contrast, if we also take into account changes in the energy band gap in J_1 (which has a $1/E_g^2$ relationship), there is a sharp drop in T_C as the particle size approaches the strong confinement regime, and this is most consistent with experimental data. The observed data generally has lower T_c values for all particle sizes compared to the calculated data. Our calculations may have errors due to our estimation of the energy gap, or possibly we have overestimated our particle size. Most significantly, based on this work, we believe that quantum effects do play an important role in determining the ferromagnetic ordering in EuS. Changes in the band gap, with concomitant changes to the magnetic properties, are important in designing spintronic devices from EuS.

Conclusions

We have synthesized a range of nanoparticle sizes to elucidate the functional relationship between particle size and the ferromagnetic ordering temperature in magnetic semiconductors. The experimental data suggest that band gap effects play a role in explaining the sharp reduction in T_C for particles whose size approaches the strong confinement regime. This provides an important link between magnetic studies of size-dependent properties in nanoparticles with what is known about the electronic properties of semiconductors with particle size.

(72) Zhao, F.; Yuan, M.; Zhang, W.; Gao, S. *J. Am. Chem. Soc.* **2006**, *128*, 11758–11759.

Acknowledgment. We thank the National Science Foundation for funding this work (NER 0304273, CAREER 0449829) and Dr. Michael Wagner of George Washington University and NSF DMR-0619260 for aid in obtaining the magnetic measurements used in the Arrott plots included in this publication.

Supporting Information Available: TGA data for $NH_2Et_2[Eu(S_2CNEt_2)_4]$, nanoparticle size histograms, electronic absorption spectra. This material is available free of charge via the Internet at http://pubs.acs.org.

CM703463S